Reentrant spin glass state induced by structural phase transition in $La_{0.4}Ce_{0.6}Co_2P_2$

Judith K. Clark,[1] Xiaoyan Tan,[1,*] V. Ovidiu Garlea,[2] Alexandra A. Arico,[1] Arthur P. Ramirez,[3] Vincent Yannello,[1]
Corey M. Thompson,[1,†] Kirill Kovnir,[4,5] and Michael Shatruk[1,‡]
[1]*Department of Chemistry and Biochemistry, Florida State University, Tallahassee, Florida 32306, USA*
[2]*Neutron Scattering Division, Oak Ridge National Laboratory, Oak Ridge, Tennessee 37831, USA*
[3]*Department of Physics, University of California at Santa Cruz, Santa Cruz, California 95060, USA*
[4]*Department of Chemistry, Iowa State University, Ames, Iowa 50011, USA*
[5]*US DOE Ames Laboratory, Ames, Iowa 50011, USA*

(Received 1 May 2020; accepted 19 June 2020; published 22 July 2020)

$La_{0.4}Ce_{0.6}Co_2P_2$ represents a borderline case in the range of solid solutions formed in the pseudobinary system $LaCo_2P_2$-$CeCo_2P_2$. The material undergoes ferromagnetic ordering at ~225 K followed by a structural collapse at ~190 K, which leads to a strong suppression of magnetization. The structural phase transition manifests itself in a gradual decrease in the parameter c and a relatively smaller increase of the parameter a of the tetragonal lattice. Interestingly, a combination of magnetic measurements and nonpolarized and polarized neutron scattering experiments suggests that the structural collapse does not lead to an antiferromagnetically ordered state, observed in samples with the higher Ce content. On the contrary, $La_{0.4}Ce_{0.6}Co_2P_2$ appears to enter a disordered, spin glass state, with gradual dissipation of the ferromagnetic ordering taking place simultaneously with the structural collapse, as evidenced by temperature-dependent measurements of the depolarization factor for a polarized neutron beam passing through the sample. The observed behavior is analogous to that reported for so-called reentrant spin glasses. In the present case, however, the appearance of the reentrant spin glass regime is caused not by tuning the chemical composition but by the structural phase transition. Electronic structure calculations confirm that the loss of magnetic ordering is caused by the subtle change to the density of states at the Fermi level due to the variation of the crystal structure of the material.

DOI: 10.1103/PhysRevMaterials.4.074412

I. INTRODUCTION

$ThCr_2Si_2$-type rare-earth cobalt phosphides, RCo_2P_2, represent a prolific group of materials, whose magnetism can be tuned over a wide range of behaviors depending on changes in the chemical composition or on external factors, such as applied pressure or magnetic field [1–4]. In recent years, the dramatic differences in the structural and magnetic properties of $LaCo_2P_2$ and the other members of the RCo_2P_2 series (R = Ce, Pr, Nd, Sm) (Fig. 1) have been leveraged to create materials that exhibit cascades of magnetic phase transitions due to the competition between different magnetically ordered states. In particular, it has been demonstrated that solid solutions $La_{1-x}Pr_xCo_2P_2$ and $La_{1-x}Nd_xCo_2P_2$ [5–8] exhibit much more complex magnetism as compared to the magnetic behavior of their ternary congeners [4].

The Ce-containing compounds, however, stand out among this family, as evidenced by the much higher antiferromagnetic (AFM) ordering temperature (T_N) of $CeCo_2P_2$ in comparison to the T_N values of $PrCo_2P_2$ or $NdCo_2P_2$ (Fig. 1). Jeitschko *et al.* reported a strong deviation in the unit-cell volume of $CeCo_2P_2$ from the gradual trend observed for the other members of the RCo_2P_2 series. Based on this observation, they proposed that the oxidation state of Ce must be close to +4.

Recently, Zhang *et al.* reported a magnetic phase diagram for the $La_{1-x}Ce_xCo_2P_2$ solid solution [9]. They established that phases with $x < 0.65$ exhibit ferromagnetic (FM) ordering of Co moments, similar to the behavior of $LaCo_2P_2$, while those with $x > 0.65$ exhibit AFM ordering, similar to $CeCo_2P_2$. They also concluded that the dramatic difference in the magnetic properties between these two regions of the phase diagram is due to the change in the Ce oxidation state from +3 for the La-rich side to +4 for the Ce-rich side of the series.

In contrast to the assumptions made by the Jeitschko and Zhang groups, our preliminary studies of the $La_{1-x}Ce_xCo_2P_2$ series by X-ray absorption near-edge structure (XANES) spectroscopy revealed the average oxidation state of Ce slightly exceeding +3, but never exceeding +3.20 [10]. Thus, it seems more plausible that these materials exhibit intermediate valence of Ce, which has been observed for many Ce-containing intermetallics [11–15]. The intermediate valence leads to itinerant behavior of the single $4f$ electron of Ce, which is usually manifested in the increased strength of the magnetic exchange and suppression of the magnetic moment on the Ce site. The latter effect frequently causes incorrect

---

[*] Present address: Department of Chemistry and Biochemistry, George Mason University, Fairfax, Virginia 22030, USA.

[†] Present address: Department of Chemistry, Purdue University, 560 Oval Drive, West Lafayette, Indiana 47907, USA.

[‡] Author to whom all correspondence should be addressed: mshatruk@fsu.edu

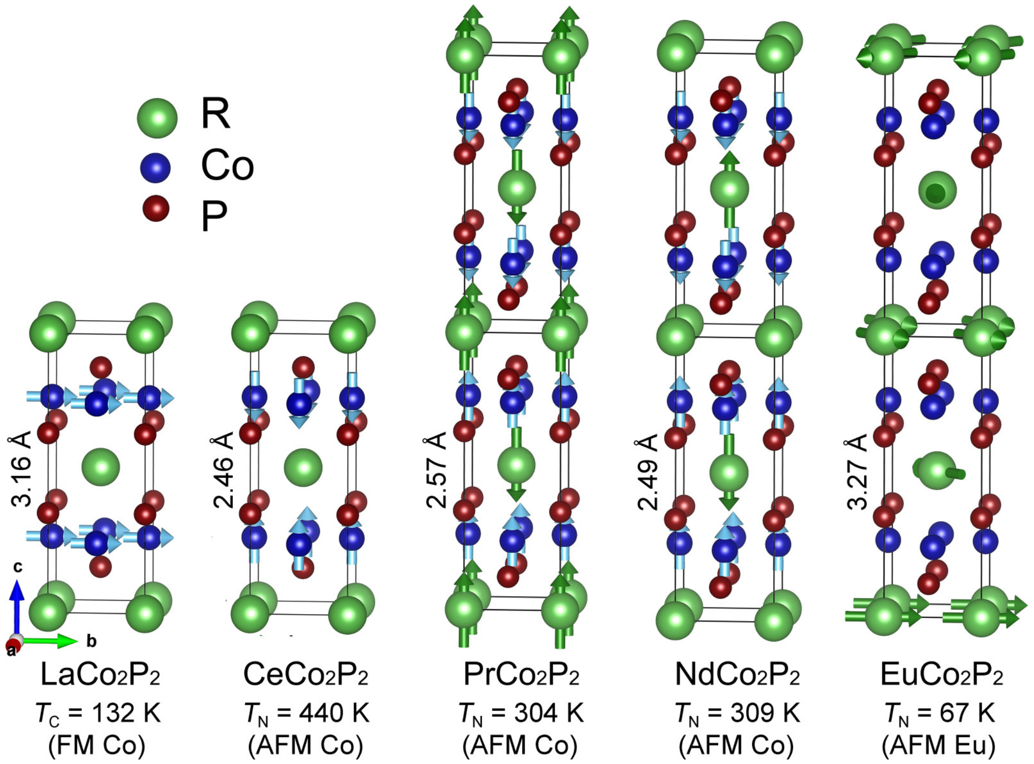

FIG. 1. The crystal and magnetic structures of RCo_2P_2, with the room-temperature P-P distances between the $[Co_2P_2]$ layers and the magnetic ordering temperatures.

assignment of the Ce oxidation state as +4 in materials that, in fact, exhibit intermediate valence.

Herein, we report a detailed investigation of the single representative of the $La_{1-x}Ce_xCo_2P_2$ series, namely the composition with $x = 0.6$, which appears at the borderline between the FM and AFM behavior. This material exhibits a temperature-induced structural collapse that leads to a dramatic change in the magnetic properties, with a possible transition into a reentrant spin glass regime. The magnetostructural phase transition has been investigated by X-ray and neutron scattering techniques, magnetic and heat capacity measurements, and electronic structure calculations. The theoretical analysis demonstrates that the structural collapse leads to a decrease in the electron density of states at the Fermi level, thus suppressing itinerant magnetic ordering in accordance with the Stoner criterion. The comprehensive experimental and theoretical study provides a plausible explanation for the unconventional magnetic behavior observed in this system.

II. EXPERIMENTAL METHODS

Starting materials. Finely dispersed powders of lanthanum (99.9%) and red phosphorus (99.999%), as well as tin shots (99.99%), were obtained from Alfa Aesar and used as received. Cobalt powder (Alfa Aesar, 99.5%) was additionally purified by heating under a flow of H_2 gas at 775 K for 5 h. Cerium powder was obtained by filing 6.4-mm-diam Ce rods (VWR, 99.9%). All manipulations during sample preparation were carried out in an argon-filled dry box (content of $O_2 <$ 1 ppm).

Synthesis. The synthesis of $La_{0.4}Ce_{0.6}Co_2P_2$ followed the tin flux method reported for $LaCo_2P_2$ [5]. The starting materials taken in the La : Ce : Co : P : Sn = 0.64 : 0.96 : 2 : 2 : 30 ratio (total mass = 5 g) were loaded in 10 mm inner diameter (i.d.) silica tubes and sealed under vacuum ($<10^{-2}$ mbar). The mixtures were annealed at 1155 K for 10 days, then cooled down to 875 K at 10 K/min and quenched in water. To remove most of the tin flux, the obtained ingot was placed in a silica tube, along with silica wool that served as a filter. The tube was heated to 625 K for 1 h, and the melted tin flux was separated from the ingot by centrifugation while hot. The remaining tin was removed by soaking the sample in dilute HCl (1:1 v/v) for 16 h. At this point, X-ray quality single crystals were selected from the sample. After the complete removal of the residual tin, the sample was washed with water and dried under suction. The phase purity of the bulk product was confirmed by powder X-ray diffraction (PXRD), which was performed on a Panalytical X'Pert Pro diffractometer using a Cu $K\alpha$ radiation source ($\lambda = 1.541\,87$ Å).

Physical measurements. Elemental analysis of select single crystals was carried out on a JEOL 5900 scanning electron microscope with an energy-dispersive X-ray (EDX) microanalysis. Magnetic measurements were performed on polycrystalline samples with a Quantum Design SQUID magnetometer MPMS-XL. Direct-current (dc) magnetic susceptibility measurements were carried out in an applied field of 10 mT in the 1.8–350 K range. Field-dependent magnetization and hysteresis were measured with the magnetic field varying from 0 to 5 T. Alternate-current (ac) magnetic susceptibility was measured with an applied field amplitude of 0.5 mT and the frequency varying from 1 to 1000 Hz. Specific heat measurements were performed with a Physical Property Measurement System (Quantum Design). To facilitate thermal equilibration, the powder sample of $La_{0.4}Ce_{0.6}Co_2P_2$ was cold-sintered with fine Ag powder, whose contribution was subtracted by using tabulated values [16].

Single-crystal X-ray diffraction (SCXRD) was carried out on a single crystal of $La_{0.4}Ce_{0.6}Co_2P_2$, which was glued with epoxy cement on the tip of a quartz fiber and mounted on a goniometer head of a Bruker AXS SMART diffractometer with an APEX-II CCD detector. The data sets were recorded as ω-scans at 0.3° step width and integrated with the Bruker SAINT software package [17]. All the data sets were indexed in the tetragonal-body-centered unit cell. The only systematic extinctions observed corresponded to the *I*-centered lattice. An analytical adsorption correction was applied using face-indexing of the crystal. Solution and refinement of the crystal structures were carried out using the SHELX suite of programs [18]. The structures were solved in the $I4/mmm$ space group (No. 139), and the final refinement was performed with anisotropic atomic displacement parameters for all atoms. The crystallographic information files (CIF) can be obtained from the Inorganic Crystal Structure Database by providing the deposition numbers 1976268–1976270.

Neutron scattering. Neutron powder diffraction (NPD) experiments were performed using the HB-2A high-resolution diffractometer at the High-Flux Isotope Reactor [19] and the POWGEN diffractometer at the Spallation Neutron Source (SNS) [20]. Data at HB-2A were collected on a sample of ~3 g held in an 8-mm-diam cylindrical vanadium container placed in a top-loading closed-cycle refrigerator, covering a temperature range of 1.7–300 K. The $\lambda = 1.539$ Å monochromatic radiation was provided by a vertically focused Ge (115) monochromator. The data were collected by scanning the detector array consisting of 44 ^{3}He tubes, to cover the total 2θ range of 7°–133° in steps of 0.05°. Neutron time-of-flight diffraction data at POWGEN were acquired using an incident neutron bandwidth centered at 1.333 Å. Data were collected at 5 K intervals on cooling the sample from 300 to 10 K. All diffraction data were analyzed by using the FULLPROF Suite Package [21].

Polarized neutron scattering measurements were carried out on a HYSPEC spectrometer at the SNS [22]. The sample, pelletized to avoid crystallite reorientation in an applied magnetic field, was loaded in a cylindrical assembly of permanent magnets that provided a vertical magnetic field of 0.4 T. The polarized incident neutron beam with $E_i = 15$ meV ($\lambda = 2.335$ Å) was obtained by reflection from a Heusler monochromator, and a Mezei flipper was used to flip the spin state of the incident neutron beam. The scattered beam was measured by a 60°-wide detector bank consisting of an array of ^{3}He linear position sensitive tubes. Flipping difference profiles were obtained at selected temperatures by successive measurements with the polarized beam parallel and antiparallel to the external magnetic field, without performing a polarization analysis of the scattered beam (using the so called "half-polarized" method). The HYSPEC instrument was also used to monitor the depolarization of the neutron beam by the sample as a function of temperature. For these measurements, an external magnetic field of only 20 Oe was applied to maintain the neutron polarization, and the polarization of the transmitted beam through the sample was analyzed using a multichannel supermirror array (a "linear polarization analysis method").

Electronic-structure calculations were performed with the tight-binding–linear muffin tin orbitals–atomic sphere approximation (TB-LMTO-ASA) software package [23]. The von Barth–Hedin exchange-correlation potential was employed for the local density approximation (LDA) calculations [24]. The radial scalar-relativistic Dirac equation was solved to obtain the partial waves. The experimentally determined crystal structure parameters (unit-cell dimensions and atomic coordinates) were used in the calculations. No empty spheres had to be added. The calculations were made for 21 952 (28 × 28 × 28) k-points in the irreducible Brillouin zone (IBZ). Integration over the IBZ was carried out using the tetrahedron method [25]. The basis set contained La($6s$, $5d$, $4f$), Co($4s$, $4p$, $3d$), and P($3s$, $3p$) orbitals, with the La($6p$) and P($3d$) functions being downfolded [26].

III. RESULTS AND DISCUSSIONS

A. Crystal structure

PXRD analysis of the bulk sample $La_{0.4}Ce_{0.6}Co_2P_2$, prepared by the Sn-flux method, confirmed the phase purity of the material, while the EDX analysis yielded the La/Ce ratio of 0.39(1):0.61(1), in good agreement with the nominal composition used for the sample preparation. The structure determination by SCXRD confirmed the $ThCr_2Si_2$-type lattice, in which the square planes of Co atoms are capped by P atoms above and below the plane, in a checkerboard fashion, and the $[Co_2P_2]$ slabs alternate with layers of La/Ce atoms along the c axis (Fig. 1). The unit-cell parameters of $La_{0.4}Ce_{0.6}Co_2P_2$ determined at 300 K were intermediate between those reported previously for $LaCo_2P_2$ and $CeCo_2P_2$ (Table I). The structure determined at 250 K showed a slight change in the unit-cell parameters, but a dramatic decrease in the c axis, by ~0.44 Å, was observed for the structure determined at 130 K. At the same time, the a axis increased only by 0.014 Å between 250 and 130 K. As a result of the much larger change in the c parameter, the unit-cell volume decreased by ~3.6%, indicating a structural collapse. Such structural transitions with the strong decrease in the c axis have been reported for a number of $ThCr_2Si_2$-type compounds [27], but they are typically induced by pressure and less frequently by the change in temperature [28–30], as observed here.

Following on this observation, we collected high-resolution NPD data for $La_{0.4}Ce_{0.6}Co_2P_2$ to obtain more accurate unit-cell parameters as a function of temperature, as well as to probe for the appearance of non-nuclear (magnetic) peaks, which were observed in the NPD pattern of the parent phase, $CeCo_2P_2$, below the AFM ordering temperature [33]. The refinement of the NPD patterns confirmed the substantial shortening of the c parameter with decreasing temperature. The decrease in the c axis and the increase in the a axis occurred rather gradually, but more pronounced changes were observed around 220, 180, and 130 K [Fig. 2(a)]. The change in the unit-cell parameters is clearly seen in the shift of a cluster of diffraction peaks, (110), (004), and (013) (Fig. 3). Importantly, however, no new peaks were observed in the

TABLE I. Crystal structure parameters of $La_{0.4}Ce_{0.6}Co_2P_2$ in comparison to parameters of $CeCo_2P_2$ and $LaCo_2P_2$.

Formula	$CeCo_2P_2$	$La_{0.4}Ce_{0.6}Co_2P_2$			$LaCo_2P_2$
T (K)	300	130	250	300	300
ICSD[a]	[31]	1976270	1976268	1976269	[32]
Unit cell a (Å)	3.8943	3.9098(2)	3.8960(6)	3.8668(1)	3.8145
c (Å)	9.598	9.7901(5)	10.230(2)	10.320(3)	11.041
V (Å^3)	145.56	149.66(1)	155.21(4)	154.31(7)	160.65
$d_{\text{P-P}}$ (Å)	2.573	2.591(1)	2.790(4)	2.850(6)	3.156
$d_{\text{Co-Co}}$ (Å)	2.752	2.765(4)	2.755(4)	2.734(6)	2.698

[a] The crystallographic information files (CIFs) can be obtained from the Inorganic Crystal Structure Database (ICSD) by referencing the registry numbers provided in the table.

NPD data, and each pattern still preserved the $I4/mmm$ space group symmetry.

The Rietveld profile analysis included anisotropic microstrain parameters [34], where the widths of the Bragg peaks were modeled by a fourth term expansion with respect to the (hkl) indices that depends on a set of parameters S_{hkl} determined by the $4/mmm$ Laue class. The hkl reflections with $l \neq 0$ are broader than the others, causing the S_{00l} strain parameters to be much larger than the S_{h00} ones. The evolution of the normalized strain parameters, S_{h00}/a and S_{00l}/c, as a function of temperature is shown in Fig. 2(b). Across the structural collapse, these strain parameters exhibit pronounced variation at the same temperatures at which the anomalies in the lattice constants are observed. Interestingly, the 300 K values are recovered below ~70 K.

The X-ray and neutron diffraction data conclusively demonstrate the occurrence of a structural phase transition below 225 K, with a dramatic collapse of the lattice along the c axis. Our results confirm an observation made by Zhang *et al.* [9], who attributed this anomalous behavior to the transition from the Ce^{3+} to the Ce^{4+} oxidation state. However, our earlier investigation of $La_{0.4}Ce_{0.6}Co_2P_2$ by XANES spectroscopy at the Ce L_3 edge showed that the average Ce oxidation state changes gradually from +3.05 at 300 K to +3.14 at 8 K [10]. In fact, we found that even in a more Ce-rich compound, $La_{0.1}Ce_{0.9}Co_2P_2$, the largest value of the Ce oxidation state does not exceed +3.2. Hence, we conclude that the solid solutions $La_{1-x}Ce_xCo_2P_2$ exhibit intermediate valence of Ce rather than the transition between the well-defined Ce^{3+} and Ce^{4+} oxidation states. While the structural collapse exerts a relatively small effect on the Ce valence in $La_{0.4}Ce_{0.6}Co_2P_2$, it leads to a dramatic change in the magnetic behavior, as demonstrated below.

B. Magnetic properties

The pure $LaCo_2P_2$ exhibits FM ordering at 132 K [5]. We have previously shown that partial substitution of Pr or Nd for La gradually increases the FM ordering temperature [5,7]. The same trend appears to hold for the FM transition in the $La_{1-x}Ce_xCo_2P_2$ series [9], but the behavior of $La_{0.4}Ce_{0.6}Co_2P_2$ is drastically different, as the temperature range in which the FM state exists is very

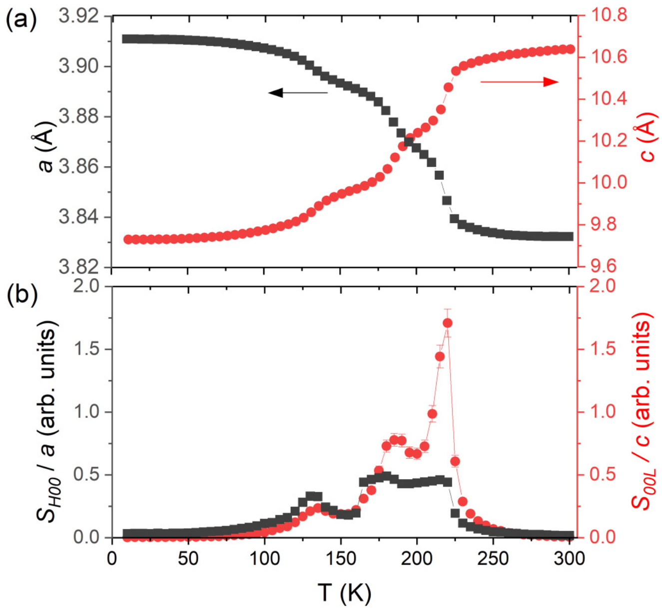

FIG. 2. Unit-cell parameters (a) and strain parameters (b) accounting for anisotropic peak broadening in the neutron powder diffraction pattern of $La_{0.4}Ce_{0.6}Co_2P_2$ as a function of temperature. The data were collected on cooling from 300 to 10 K at 5 K intervals.

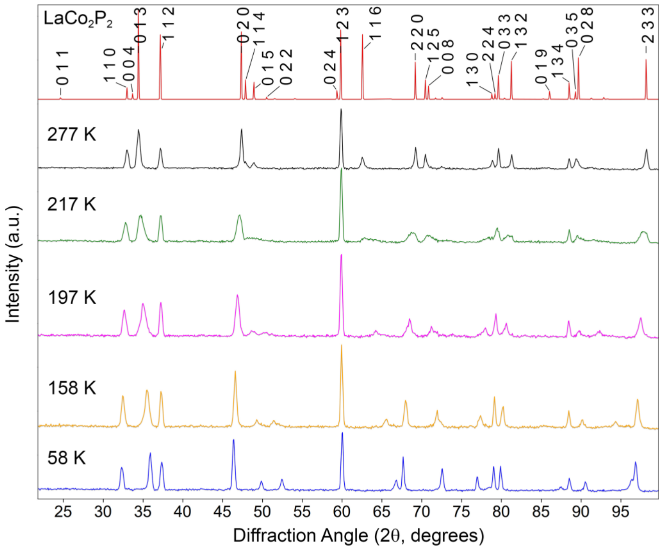

FIG. 3. Experimental neutron powder diffraction patterns of $La_{0.4}Ce_{0.6}Co_2P_2$ collected at different temperatures, in comparison to the pattern calculated from the crystal structure at 300 K.

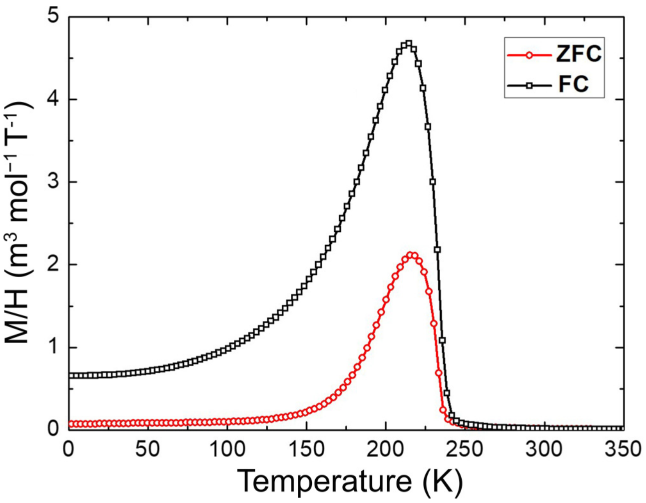

FIG. 4. Temperature dependence of FC and ZFC magnetization measured on a powder sample of $La_{0.4}Ce_{0.6}Co_2P_2$ under an applied magnetic field of 10 mT.

narrow. The dc magnetization measured on a polycrystalline sample of $La_{0.4}Ce_{0.6}Co_2P_2$ in the field-cooled (FC) and zero-field-cooled (ZFC) modes showed an abrupt increase around 235 K, followed by a pronounced maximum at 215 K and a drop below that temperature (Fig. 4). The character of the magnetization curves suggests the initial FM ordering followed by AFM ordering, which also coincides with the structural collapse (Fig. 2). Nevertheless, the NPD data do not provide any evidence for AFM ordering, as no additional (magnetic) peaks were observed in the NPD patterns recorded below 215 K (Fig. 3). Any significant shifts in the nuclear peak positions are only related to the change in the unit-cell parameters as a function of temperature.

To get further insight into the unusual magnetic behavior below 215 K, we carried out isothermal magnetization measurements between 250 and 100 K, at 5 to 10 K increments [Fig. 5(a)]. Typical paramagnetic behavior was observed at 250 and 240 K. The isotherms recorded from 230 to 190 K showed a rapid initial increase in magnetization at lower applied fields, followed by a more gradual growth as the field was increased. This behavior is in agreement with the emergence of FM ordering. The maximum magnetization value was observed for the 220 K isotherm. Upon cooling to 180 K, the isotherm became strongly suppressed, with a slower increase at low fields and a linear growth at higher fields. This behavior remained consistent in all isotherms recorded below 180 K, and the maximum magnetization value reached at 5 T continued to decrease as the temperature was lowered. This dramatic change in the magnetization behavior is also reflected in the character of the Arrott plot [Fig. 5(b)], which indicates that the T_C value falls in the 225–230 K range. As the temperature is decreased below T_C, crossing of Arrott isotherms is observed, in agreement with the suppression of magnetization at lower temperatures.

We also carried out specific heat, $C(T)$, measurements on a pellet of $La_{0.4}Ce_{0.6}Co_2P_2$, which was pressed with an addition of a small amount of silver, to improve thermal equilibration. A weak anomaly observed at ∼225 K (Fig. 6) is in agreement

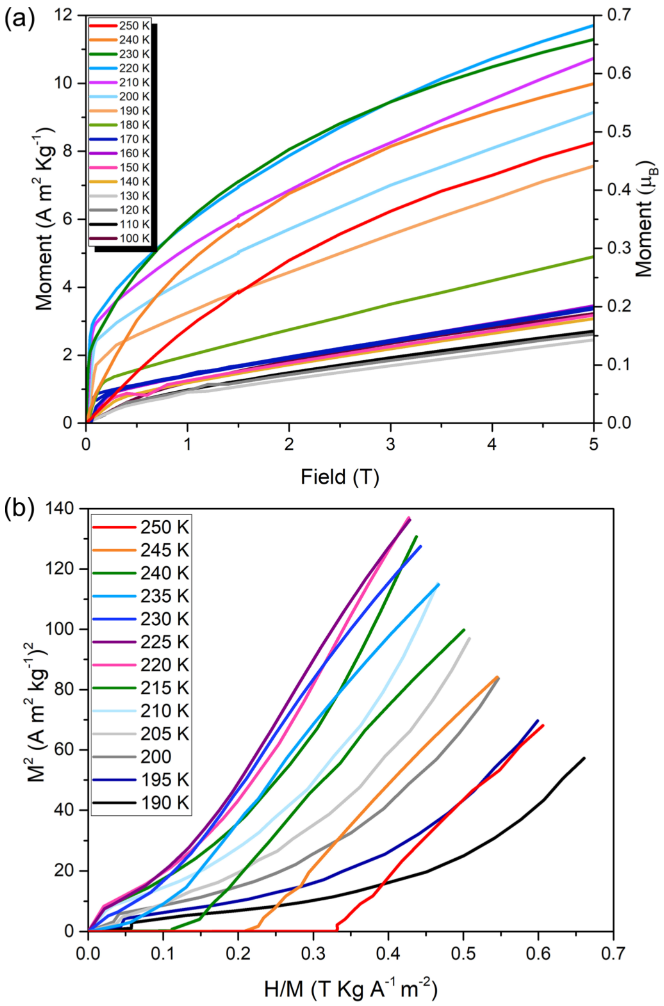

FIG. 5. Isothermal magnetization curves (a) and the Arrott plot (b) for a powder sample of $La_{0.4}Ce_{0.6}Co_2P_2$. The magnetization values are expressed per formula unit.

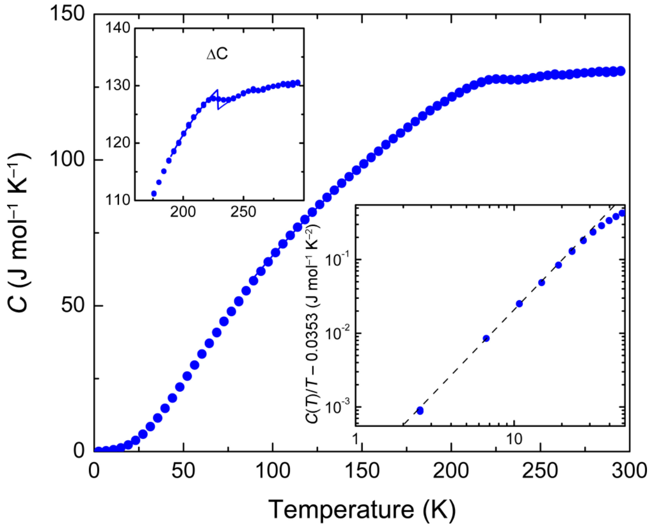

FIG. 6. Temperature dependence of specific heat measured on a pressed pellet of $La_{0.4}Ce_{0.6}Co_2P_2$. The first inset shows an enlarged view of the jump around 225 K, while the second inset shows the fit to the equation discussed in the text: $C(T) = \gamma T + \beta T^{\alpha}$.

with the FM phase transition. No other significant features were observed in the $C(T)$ curve at lower temperatures. Below 30 K, the data can be fit by the form $C(T) = \gamma T + \beta T^{\alpha}$, where $\gamma = 35.3\,\mathrm{mJ/(mol\,K^2)}$, $\beta = \mathrm{J/(mol\,K^{3.3})}$, and $\alpha = 2.3$ (Fig. 6, inset). The term "linear in T" originates from the combination of Sommerfeld and spin-glass [35] contributions, while the power law of the second term suggests excitations due to the combined effects of both magnetic and lattice modes.

C. Polarized neutron scattering

The field-dependent magnetization observed below 180 K suggest substantial AFM exchange interactions, but the NPD data indicate a lack of long-range AFM ordering. At the same time, the NPD pattern recorded at 217 K did not reveal any notable contribution to the nuclear peak intensities from the FM ordered magnetic moments of Co, due to the low value of the ordered magnetic moment. The moment per Co atom estimated from the value of magnetization at 220 K and 5 T is only ∼0.34 μ_B. This moment value is similar to the saturation moment per Co atom observed for $\mathrm{LaCo_2P_2}$ (0.43 μ_B) [5]. To evaluate the moments on the Co and Ce sites more accurately, we employed the polarized neutron flipping difference method, which takes advantage of the interference term between the nuclear and magnetic signals ($F_M F_N$) and offers a much higher sensitivity to FM ordered moments [36,37]. Moreover, taking the difference between signals recorded with the spin of the incident neutron beam aligned parallel and antiparallel to the magnetic field direction eliminates all of the nonmagnetic background.

Polarized neutron spectroscopy experiments carried out at HYSPEC showed the lack of any magnetic signal at 280 K and a clear signature of FM ordering in the spectrum recorded at 210 K (Fig. 7). At 150 K, however, the FM signal became substantially suppressed and essentially vanished at 50 K. The 210 K spectrum was successfully fit with a soft FM model where magnetic moments align parallel to the applied magnetic field, regardless of the crystal grain orientation. The model fit, shown as a red line in Fig. 7(b), yields an ordered moment of $0.15(1)\mu_B$ per Co atom and negligible $-0.01(1)\mu_B$ per Ce atom. These values are in good agreement with the total magnetization of 0.18 μ_B observed in the 210 K isotherm at ∼0.4 T [Fig. 5(a)]; this field value is equivalent to that provided by the permanent magnetic yoke used in the neutron experiment.

The emergence and loss of FM ordering as a function of temperature were followed by measuring the relative depolarization of the polarized neutron beam as it passed through a pelletized powder of $\mathrm{La_{0.4}Ce_{0.6}Co_2P_2}$. The depolarization was evaluated from the change in the intensity of the spin-flip signal (I^+–I^-), which is sensitive only to the magnetism in the sample [38]. The measurements were performed with a vertical guide field of 20 Oe, and the spin-flip was analyzed using a supermirror array. The beam depolarization factor was normalized to the value measured at room temperature in the paramagnetic state, where no effect on the beam transmission is expected. The depolarization increases abruptly at ∼235 K, in agreement with the onset of FM ordering of the sample. Below 190 K, the depolarization factor steadily decreases as the sample magnetization vanishes, and it plateaus to a value of ∼5% below 110 K. Thus, the temperature dependence of the depolarization factor suggests the gradual loss of FM ordering caused by the structural collapse, in general agreement with the observations made from magnetic measurements. As shown in earlier studies, reduction of depolarization can also be due to a spatial and size redistribution of the magnetic domains in the sample [39,40]. Nevertheless, the flipping difference results suggest that in $\mathrm{La_{0.4}Ce_{0.6}Co_2P_2}$ the evolution of the depolarization is mainly due to the decay of the spin-spin correlation length associated with the structural collapse.

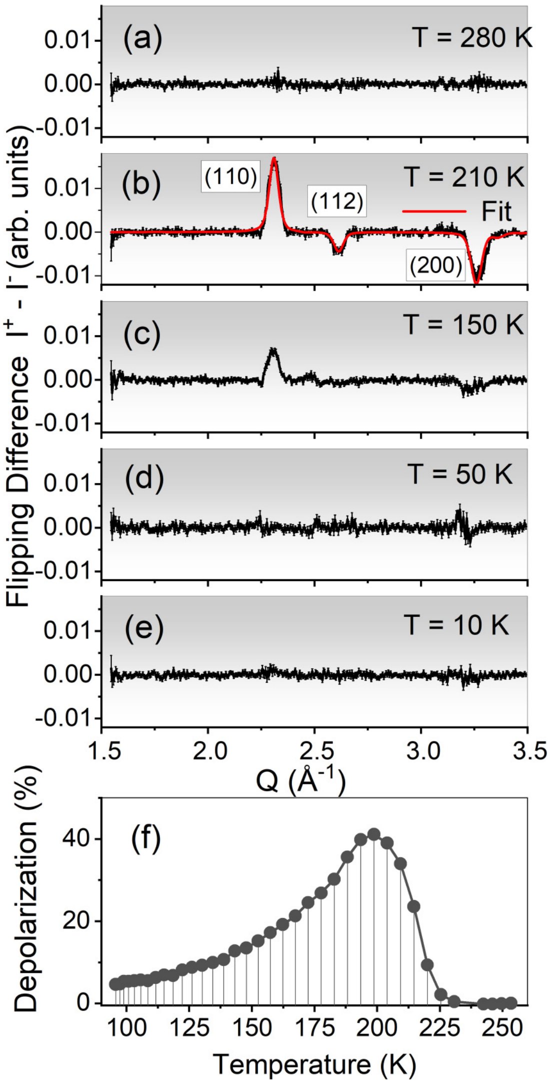

FIG. 7. (a)–(e) The flipping difference of neutron scattering ($I^+ - I^-$) recorded on a powder sample of $\mathrm{La_{0.4}Ce_{0.6}Co_2P_2}$ at different temperatures. (f) The temperature dependence of the neutron depolarization factor by the sample.

D. Reentrant spin glass behavior

Based on the observations made from the nonpolarized and polarized neutron scattering experiments, we can conclude that $\mathrm{La_{0.4}Ce_{0.6}Co_2P_2}$ gradually loses long-range FM ordering below 190 K. Given the substantial divergence between the FC and ZFC magnetization in this temperature range (Fig. 4), one might consider the existence of a frozen disordered state with short-range AFM correlations, i.e., the spin glass (SG). Such behavior received a somewhat incorrect but sufficiently accepted [41] name, i.e., "reentrant spin glass" (RSG), reflecting the successive transition from the disordered PM state to the ordered FM state and then again to the disordered SG state [42,43]. A common approach to verify the formation of the spin glass state is to measure magnetic susceptibility at different frequencies of an applied ac field, to observe the frequency dependence of the maximum in the ac susceptibility at the spin-freezing temperature, T_g [44]. This approach, however, was devised for the systems that transition from the *disordered* PM to the frozen and *disordered* SG state. In the present case, $La_{0.4}Ce_{0.6}Co_2P_2$ transitions from the FM ordered state to the RSG state as the temperature is lowered, and the FM ordering is lost gradually (Fig. 4), suggesting that the structural collapse causes dissociation of the long-range-ordered FM structure into smaller FM clusters, in line with the theoretical scenario proposed by Gabay and Toulouse [45]. Therefore, the dynamics at the phase boundary can be rather slow. The gradual dissipation of the FM ordered state, with the decay of the spin-spin correlation length, is well supported by the temperature-dependent changes in the neutron depolarization factor, as shown in Fig. 7(f).

AC measurements revealed a strong peak in the temperature-dependent magnetization (M') at ~226 K, with a very weak frequency dependence (Fig. 8). We attribute this peak to the initial FM ordering confirmed by the magnetic measurements, polarized neutron scattering, and heat capacity measurements. The Mydosh parameter [44] calculated from the frequency dependence of the peak maximum was $\varphi = 0.002$, which falls outside the range typically observed for spin glasses (0.004–0.08). This value supports the existence of an ordered FM state with some degree of glassiness. There is also a shoulder observed at ~180 K, which coincides with the onset of the structural collapse and the gradual loss of the FM ordering. Unfortunately, the shoulder is poorly defined for accurate calculation of the Mydosh parameter, but it clearly indicates the onset of a gradual transition to a different magnetic state.

The loss of the long-range FM ordered state observed in $La_{0.4}Ce_{0.6}Co_2P_2$ is similar to the behavior reported for other RSG systems, such as $Au_{0.82}Fe_{0.18}$, $Fe_{0.7}Al_{0.3}$, $Ce(Fe_{0.96}Ru_{0.04})_2$, and $(Ni/Fe)_{0.25}Au_{0.75}$ [46–48]. ac susceptibility measurements performed on the latter system also revealed that the initial strong peak caused by FM ordering was followed by a weaker shoulder, attributed to the transition to the RSG state [49]. A distinct feature of $La_{0.4}Ce_{0.6}Co_2P_2$, however, is the coincidence of the loss of FM ordering with the gradual structural collapse that leads to a dramatic decrease in the lattice volume. This is an example of the transition from the FM to RSG state caused by the temperature-induced structural phase transition. As we show in the next section, the structural collapse intensifies the competition between the FM and AFM exchange interactions, thus promoting spin frustration and the transition to the RSG state.

We recall that powder diffraction study indicated that the sample crystallinity was found to recover at low temperatures. Thus, the persistence of the glassy state beyond the structural collapse regime supports the hypothesis that it originates primarily from the competing magnetic interaction rather than from the lattice disorder.

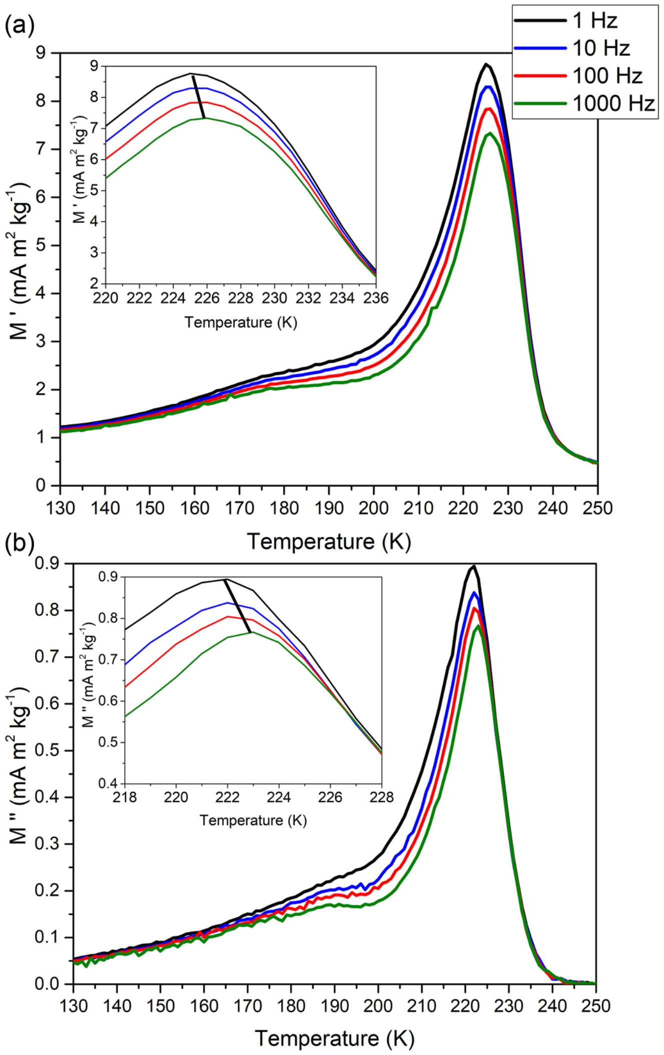

FIG. 8. The real (a) and imaginary (b) parts of magnetization measured on a powder sample of $La_{0.4}Ce_{0.6}Co_2P_2$ under ac magnetic field with an amplitude of 0.5 mT and variable frequency. The insets show an enlarged view of the peak observed around 225 K.

E. Electronic structure

The electronic density of states (DOS) of $La_{0.4}Ce_{0.6}Co_2P_2$ was calculated using the structural parameters obtained from the SCXRD measurements but assuming that the rare-earth site is occupied only by La. We do not expect La or Ce to impact substantially magnetic coupling within the Co sublattice, which is primarily responsible for the FM ordering emerging below ~230 K. Hence, such a model avoids complications that arise due to the itinerancy of the Ce 4f electrons while providing an adequate description of the electronic structure of the Co 3d subband, primarily responsible for the itinerant magnetism in this type of materials [1].

The structural parameters obtained at 300 and 130 K were taken to represent the normal and collapsed structures, respectively. Nonpolarized electronic-structure calculations revealed that in both structures the Fermi level crosses a

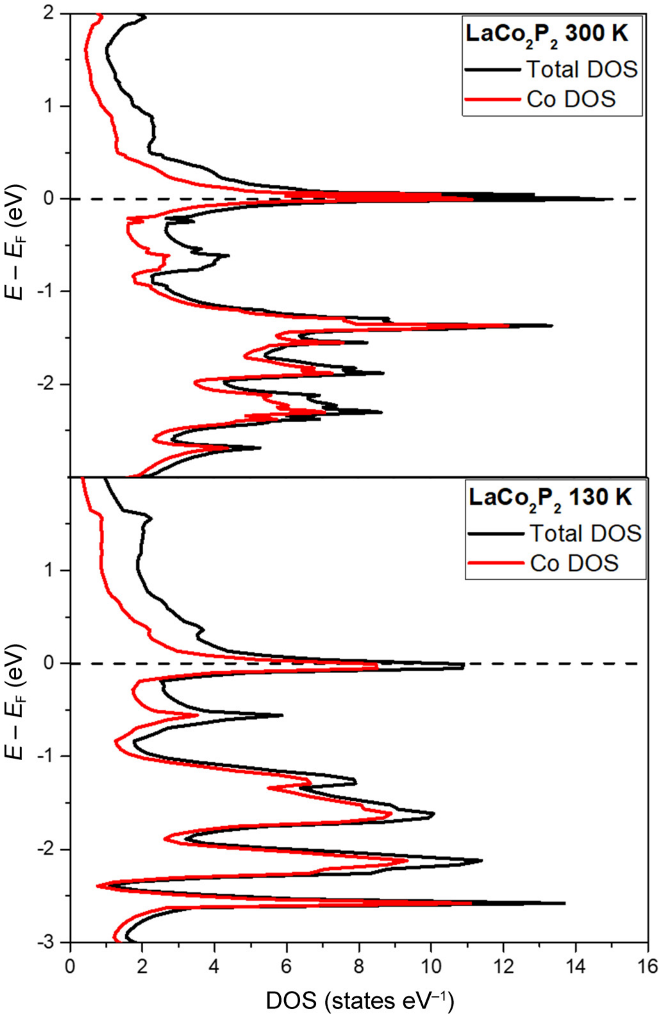

FIG. 9. Nonpolarized density of states calculated for the model structure of $LaCo_2P_2$ using the unit-cell parameters of $La_{0.4}Ce_{0.6}Co_2P_2$ at 300 and 130 K. The Fermi level is indicated with a dashed horizontal line.

strong DOS peak, but the positioning of the peak with respect to the Fermi energy (E_F) is slightly different (Fig. 9). The transition to the collapsed structure lowers the DOS at the Fermi level, $n(E_F)$. The Stoner product, $In(E_F)$, was evaluated by approximating the Co-Co exchange constant (I) with a value established for the Co metal [5,50–52]. The product decreased from 1.2 in the normal structure to 0.84 in the collapsed one, justifying the observed loss of FM ordering caused by the structural phase transition in $La_{0.4}Ce_{0.6}Co_2P_2$. We note that, while the use of the I value of the elemental Co is a rough approximation, it does not impact the main conclusion of these calculations: the Stoner product is substantially decreased in the collapsed structure due to the lowering of the $n(E_F)$ value.

IV. CONCLUDING REMARKS

In summary, we have provided sufficient evidence to demonstrate that $La_{0.4}Ce_{0.6}Co_2P_2$ represents a borderline behavior in the series of solid solutions $La_{1-x}Ce_xCo_2P_2$. At this composition, the competition between the normal and collapsed $ThCr_2Si_2$-type structures and between the FM and AFM ordering in the Co sublattice causes the emergence of reentrant spin glass (RSG) behavior below 190 K. This RSG state is induced by a temperature-driven structural collapse of the FM state that settles below 225 K and thus exists in a rather narrow temperature interval. It is interesting to ponder on the nature of this magnetostructural coupling. The fact that the FM ordering develops quite rapidly while the structural collapse and the loss of FM state proceed much more gradually with temperature suggests that the FM ordering might be the trigger for the structural phase transition. Indeed, we have previously reported that FM ordering in this class of materials leads to an increase in the Co-Co separation in the *ab* plane, which induces a compensating decrease in the P-P distances along the *c* axis [5,6,53]. It can be speculated that a similar effect takes place in $La_{0.4}Ce_{0.6}Co_2P_2$: as can be seen from our structural data, the lengthening of Co-Co distances due to FM ordering at 225 K triggers the initial shortening of the *c* axis, which then propagates into the gradual structural collapse that impacts the density of states at the Fermi level and leads to the loss of Stoner ferromagnetism with the simultaneous appearance of the RSG state. Given all these considerations, it is of interest to investigate other members of the $La_{1-x}Ce_xCo_2P_2$ series, as they may offer further support to this hypothesis.

ACKNOWLEDGMENTS

This work was supported by the National Science Foundation (awards DMR-1905499 to M.S. and DMR- 1534741 to A.P.R.). A portion of this research used resources at the High Flux Isotope Reactor and Spallation Neutron Source, DOE Office of Science User Facilities operated by the Oak Ridge National Laboratory.

[1] X. Tan, Z. P. Tener, and M. Shatruk, Acc. Chem. Res. **51**, 230 (2018).
[2] X. Tan *et al.*, J. Am. Chem. Soc. **138**, 2724 (2016).
[3] M. Chefki, M. M. Abd-Elmeguid, H. Micklitz, C. Huhnt, W. Schlabitz, M. Reehuis, and W. Jeitschko, Phys. Rev. Lett. **80**, 802 (1998).
[4] M. Reehuis and W. Jeitschko, J. Phys. Chem. Solids **51**, 961 (1990).
[5] K. Kovnir, C. M. Thompson, H. D. Zhou, C. R. Wiebe, and M. Shatruk, Chem. Mater. **22**, 1704 (2010).
[6] K. Kovnir, C. M. Thompson, V. O. Garlea, D. Haskel, A. A. Polyanskii, H. D. Zhou, and M. Shatruk, Phys. Rev. B **88**, 104429 (2013).
[7] C. M. Thompson, K. Kovnir, V. O. Garlea, E. S. Choi, H. D. Zhou, and M. Shatruk, J. Mater. Chem. C **2**, 7561 (2014).
[8] X. Y. Tan *et al.*, Phys. Rev. B **95**, 024428 (2017).

[9] Y. Tian, Y. Kong, K. Liu, A. Zhang, R. He, and Q. Zhang, Physica B **512**, 75 (2017).

[10] A. P. Menushenkov, A. A. Yaroslavtsev, O. V. Grishina, R. V. Chernikov, A. A. Arico, C. M. Thompson, K. Kovnir, and M. Shatruk, Solid State Phenom. **190**, 200 (2012).

[11] E. A. Goremychkin *et al.*, Science **359**, 186 (2018).

[12] J. Lawrence and D. Murphy, Phys. Rev. Lett. **40**, 961 (1978).

[13] M. Nicklas *et al.*, Phys. Rev. Lett. **109**, 236405 (2012).

[14] A. R. Mackintosh, Physica B+C **130**, 112 (1985).

[15] X. Y. Tan, V. O. Garlea, P. Chai, A. Y. Geondzhian, A. A. Yaroslavtsev, Y. Xin, A. P. Menushenkov, R. V. Chernikov, and M. Shatruk, J. Solid State Chem. **236**, 147 (2016).

[16] E. S. Domalski and E. D. Hearing, in *NIST Chemistry WebBook, NIST Standard Reference Database Number 69*, edited by P. J. Linstrom and W. G. Mallard (National Institute of Standards and Technology, Gaithersburg, MD, 2020).

[17] *SMART and SAINT* (Bruker AXS, Madison, WI, 2007).

[18] G. M. Sheldrick, Acta Crystallogr. Sect. C **71**, 3 (2015).

[19] V. O. Garlea, B. C. Chakoumakos, S. A. Moore, G. B. Taylor, T. Chae, R. G. Maples, R. A. Riedel, G. W. Lynn, and D. L. Selby, Appl. Phys. A **99**, 531 (2010).

[20] M. Kirkham, L. Heroux, M. Ruiz-Rodriguez, and A. Huq, Rev. Sci. Instr. **89**,092904 (2018).

[21] J. Rodríguez-Carvajal, Physica B **192**, 55 (1993).

[22] B. Winn *et al.*, EPJ Web Conf. **83**, 03017 (2015).

[23] R. Tank, O. Jepsen, A. Burkhardt, and O. K. Andersen, *The Program TB-LMTO-ASA. Version 4.7* (Max-Planck-Institut fur Festkorperforschung, Stuttgart, 1999).

[24] U. Von Barth and L. Hedin, J. Phys. C **5**, 1629 (1972).

[25] P. E. Blochl, O. Jepsen, and O. K. Andersen, Phys. Rev. B **49**, 16223 (1994).

[26] W. R. L. Lambrecht and O. K. Andersen, Phys. Rev. B **34**, 2439 (1986).

[27] M. Shatruk, J. Solid State Chem. **272**, 198 (2019).

[28] C. Huhnt, G. Michels, M. Roepke, W. Schlabitz, A. Wurth, D. Johrendt, and A. Mewis, Physica B **240**, 26 (1997).

[29] V. Keimes, D. Johrendt, A. Mewis, C. Huhnt, and W. Schlabitz, Z. Anorg. Allg. Chem. **623**, 1699 (1997).

[30] F. Ronning, E. D. Bauer, T. Park, S. H. Baek, H. Sakai, and J. D. Thompson, Phys. Rev. B **79**, 134507 (2009).

[31] W. Jeitschko, U. Meisen, M. H. Möller, and M. Reehuis, Z. Anorg. Allg. Chem. **527**, 73 (1985).

[32] M. Reehuis, C. Ritter, R. Ballou, and W. Jeitschko, J. Magn. Magn. Mater. **138**, 85 (1994).

[33] M. Reehuis, W. Jeitschko, G. Kotzyba, B. Zimmer, and X. Hu, J. Alloys Compd. **266**, 54 (1998).

[34] P. Stephens, J. Appl. Cryst. **32**, 281 (1999).

[35] P. W. Anderson, B. I. Halperin, and C. M. Varma, Philos. Mag. A **25**, 1 (1972).

[36] E. Lelièvre-Berna *et al.*, Meas. Sci. Technol. **21**, 055106 (2010).

[37] O. Rivin, H. Shaked, A. Gukasov, and E. a. N. Caspi, J. Neutron Res. **18**, 13 (2015).

[38] R. M. Moon, T. Riste, and W. C. Koehler, Phys. Rev. **181**, 920 (1969).

[39] Y. Endoh, Prog. Theor. Phys. Suppl. **101**, 567 (1990).

[40] S. G. E. te Velthuis, N. H. van Dijk, M. T. Rekveldt, J. Sietsma, and S. van der Zwaag, J. Appl. Phys. **89**, 1275 (2000).

[41] A Web of Science search for "reentrant spin glass" results in ~700 references spanning the period from 1980 to the present.

[42] B. R. Coles and S. B. Roy, in *Frontiers in Solid State Sciences*, edited by L. C. Gupta and M. S. Multani, Vol. 2 (World Scientific, 1993), pp. 363–371.

[43] B. R. Coles, Philos. Mag. B **49**, L21 (1984).

[44] J. A. Mydosh, *Spin Glasses: An Experimental Introduction* (Taylor & Francis, Washington, DC, 1993).

[45] M. Gabay and G. Toulouse, Phys. Rev. Lett. **47**, 201 (1981).

[46] S. B. Roy and M. K. Chattopadhyay, Phys. Rev. B **79**, 052407 (2009).

[47] M. Shiga, Y. Muraoka, and Y. Nakamura, J. Magn. Magn. Mater. **54–57**, 187 (1986).

[48] M. K. Chattopadhyay, S. B. Roy, and P. Chaddah, Phys. Rev. B **72**, 180401(R) (2005).

[49] A. Chakravarti, R. Ranganathan, and C. Bansal, Solid State Commun. **82**, 591 (1992).

[50] J. F. Janak, Phys. Rev. B **16**, 255 (1977).

[51] G. D. Samolyuk and G. J. Miller, J. Comput. Chem. **29**, 2177 (2008).

[52] K. Kovnir, W. M. Reiff, A. P. Menushenkov, A. A. Yaroslavtsev, R. V. Chernikov, and M. Shatruk, Chem. Mater. **23**, 3021 (2011).

[53] V. Yannello *et al.*, Chem. Eur. J. **25**, 5865 (2019).